The morphology of the thermal Sunyaev-Zel'dovich sky

Article (Published Version)

Monthly Notices
of the
ROYAL ASTRONOMICAL SOCIETY

Mon. Not. R. Astron. Soc. **419,** 138–152 (2012) doi:10.1111/j.1365-2966.2011.19679.x

The morphology of the thermal Sunyaev–Zel'dovich sky

Dipak Munshi,[1⋆] Joseph Smidt,[2] Shahab Joudaki[2] and Peter Coles[1]

[1]*School of Physics and Astronomy, Cardiff University, Queen's Buildings, 5 The Parade, Cardiff CF24 3AA*
[2]*Department of Physics and Astronomy, University of California, Irvine, CA 92697, USA*

Accepted 2011 August 22. Received 2011 August 1; in original form 2011 May 27

ABSTRACT

At high angular frequencies, beyond the damping tail of the primary cosmic microwave background (CMB) power spectrum, the thermal Sunyaev–Zel'dovich (tSZ) effect constitutes the dominant signal in the CMB sky. The tSZ effect is caused by large-scale pressure fluctuations in the baryonic distribution in the universe, such that its statistical properties provide estimates of corresponding properties of the projected 3D pressure fluctuations. The power spectrum of the tSZ is a sensitive probe of the amplitude of density fluctuations, and the bispectrum can be used to separate the bias associated with the pressure. The bispectrum is typically probed with its one-point real-space analogue, the skewness. In addition to the ordinary skewness the morphological properties, as probed by the well-known Minkowski functionals, also require the generalized one-point statistics, which at the lowest order are identical to the generalized skewness parameters. The concept of generalized skewness parameters can be further extended to define a set of three associated generalized *skew-spectra*. We use these skew-spectra to probe the morphology of the tSZ sky or the y-sky. We show how these power spectra can be recovered from the data in the presence of an arbitrary mask and noise templates using the well known pseudo-C_l approach for arbitrary beam shape. We also employ an approach based on the halo model to compute the tSZ bispectrum. The bispectrum from each of these models is then used to construct the generalized skew-spectra. We consider the performance of an all-sky survey with *Planck*-type noise and compare the results against a noise-free ideal experiment using a range of smoothing angles. We find that the skew-spectra can be estimated with very high signal-to-noise ratio from future frequency-cleaned tSZ maps that will be available from experiments such as *Planck*. This will allow their *mode-by-mode* estimation for a wide range of angular frequencies l and will help us distinguish them from other sources of non-Gaussianity.

Key words: methods: analytical – methods: numerical – methods: statistical – cosmology: theory.

1 INTRODUCTION

Measurements of cosmological parameters from cosmic microwave background (CMB) surveys such as those performed by satellite missions like *Wilkinson Microwave Anisotropy Probe* (*WMAP*)[1] and *Planck*[2] not only provide a very accurate picture of the background geometry and dynamics of the universe but can also reveal much more detailed information about ongoing physical processes. Indeed, with all-sky coverage and wide range of previously uncharted frequencies, the data provided by experiments such as *Planck* will produce 'secondary' science which is arguably as valuable as the 'primary' science; see e.g. Aghanim, Majumdar & Silk (2008) for a recent review. In any event, accurate modelling of secondary non-Gaussianities is required to avoid 20–30 per cent constraint degradations in future CMB data sets such as *Planck* and *CMBPol*[3] (Smidt et al. 2010).

The large-scale properties of hot intergalactic gas can be probed through multifrequency observations. Inverse-Compton scattering of CMB photons known as thermal Sunyaev–Zel'dovich (tSZ) effect leaves a characteristic distortion pattern in the CMB spectrum (Sunyaev & Zel'dovich 1972, 1980; Rephaeli 1995; Birkinshaw 1999). The fluctuation of this distortion across the sky as probed by CMB observations can provide valuable clues to the fluctuations of the gas density and temperature. In the (low frequency) Rayleigh–Jeans (RJ) regime it produces

⋆E-mail: dipak.munshi@astro.cf.ac.uk
[1] http://wmap.gsfc.nasa.gov/
[2] http://www.rssd.esa.int/Planck
[3] http://cmbpol.uchicago.edu/

constant decrement, while there is an increment at high frequencies; in between there is a null (around 217 GHz). This characteristic behaviour is a potential tool for the separation of tSZ from the other contributions to the temperature anisotropy. Based on accurate knowledge of the tSZ and CMB spectrum, foreground removal techniques have been developed to isolate the tSZ signal in the presence of primary anisotropy and instrumental noise. These techniques are extremely effective in the subtraction of primary anisotropies due to its well understood (perfect blackbody) frequency dependence and almost exactly Gaussian statistical behaviour (Bouchet & Gispert 1999; Cooray, Hu & Tegmark 2000; Delabroullie, Cardoso & Patanchon 2003; Leach et al. 2008; Veneziani et al. 2009; Joudaki et al. 2010). The tSZ effect is now routinely imaged in massive individual galaxy clusters where the temperature of the scattering medium can reach 10 keV. This effect produces a change in CMB temperature of order 1 mK at RJ wavelengths. Individual galaxy cluster tSZ images have a variety of astrophysical and cosmological applications including direct measurement of the angular diameter distance to the cluster through a combined analysis of X-ray data and measurement of the gas mass, which can be useful in the estimation of the baryon fraction of the universe. The High Frequency Instrument (HFI) of *Planck*, in particular, has been designed with bands centred at the minimum, the null and the maximum of the tSZ emission. The extraction of frequency-cleaned CMB and tSZ maps of a catalogue of galaxy clusters selected by their tSZ effect is part of the scientific program of *Planck*. Here we are moreover interested in the general intergalactic medium (IGM) where the gas is expected to be at $\leq$1 keV in mild overdensities, which leads to CMB contributions in the μK range. In this work, we primarily focus on the statistical study of wide-field CMB data where tSZ effects lead to anisotropies in the temperature distribution due to both resolved and unresolved galaxy clusters, keeping in mind that the tSZ contribution is the dominant signal beyond the damping tail of the primary anisotropy power spectrum. We focus on analytical modelling of morphological properties of the tSZ fluctuations using Minkowski functionals (MFs).

Modelling of the lower order statistics of the tSZ effect can be performed using either analytical or numerical approaches. Authors using analytical approaches (Cooray 2000, 2001b; Seljak 2000; Zhang & Pen 2001; Komatsu & Seljak 2002; Zhang & Seth 2007) have generally used the halo model (Cooray & Seth 2002). To trace the tSZ effect due to photoionized gas outside of collapsed haloes, see e.g. Cooray (2001b). A second-order perturbative formalism is used to model the bispectrum in this approach. The gas will typically be at a temperature similar to the ionization energy of hydrogen and helium. The bias associated with the pressure fluctuations is assumed to be redshift dependent. As for the tSZ effect from material within collapsed haloes, the shock-heated gas is typically assumed to be in hydrodynamic equilibrium in virialized haloes. The statistical description of haloes that include the number count distribution is assumed to be described by the Press–Schechter formalism (Press & Schechter 1974). The radial profile of such haloes is assumed to be that of NFW (Navarro, Frenk & White 1996). These ingredients are sufficient for modelling of the tSZ effect from collapsed haloes (Cooray 2000).

In addition to analytical modelling, numerical simulations of tSZ play an important role in our understanding of the physics involved (Persi et al. 1995; Cen & Ostriker 1999; da Silva et al. 2000; Refregier et al. 2000; Seljak, Burwell & Pen 2001; Springel, White & Hernquist 2001; Refregier & Teyssier 2002; White, Hernquist & Springel 2002; Lin et al. 2004; Zhang, Pen & Trac 2004; Cao, Liu & Fang 2007; Hallman et al. 2007, 2009; Roncarelli et al. 2007). Some of these studies incorporate complications from additional gas physics such as radiative cooling, pre-heating and supernova (SN)/active galactic nucleus (AGN) feedback, at least to a certain extent. The inputs are otherwise difficult to incorporate in any analytical calculation. On the other hand, the simulations are limited in their dynamic range and can benefit from analytical insights.

The tSZ power spectrum is known to be a sensitive probe of the amplitude of density fluctuations. Higher order statistics, such as the skewness or the bispectrum we study here, can provide independent estimates of the bias associated with the baryonic pressure. Typically, a collapsed three-point statistics such as the (one-point) skewness is employed for this purpose. The skewness compresses all available information in the bispectrum. The recently proposed skew-spectrum is a power spectrum associated with the bispectrum (Munshi & Heavens 2010), which is useful to probe non-Gaussianity as a function of scale or the harmonics l. In addition to the lower order multispectra, morphological statistics such as the MFs carry independent information of non-Gaussianity and have been studied extensively in the literature (Hikage et al. 2002, 2003b, 2008; Hikage, Taruya & Suto 2003a; Hikage, Komatsu & Matsubara 2006). At the lowest order, the MFs are completely described by a set of three different skewness parameters that describe a complete set of three MKs in 2D. We have extended these generalized skewness parameters to their corresponding skew-spectra. The skew-spectra sample the bispectra with varying weights and carry independent information. The estimation of these skew-spectra can be done at relatively modest computational cost. The skew-spectra can be constructed by cross-correlating suitable maps that are constructed from the original (frequency-cleaned) tSZ maps. The construction involves differential operations on beam smoothed pixelized maps that can also be performed in the harmonic domain. The estimators for skew-spectra can be constructed following the general principle of power spectrum estimation. We use the well-known pseudo-C_l (PCL) approach developed by Hivon et al. (2002). It can handle arbitrary sky coverage and arbitrary noise characteristics and beam patterns. We use the PCL approach to construct the variance in the estimators as well as to compute their cross-correlations. These results are accurate for surveys with all-sky coverage and can also be modified to take into account partial sky coverage, using the flat sky approximation.

In relating to the experimental scenarios we will consider an experimental set-up similar to the ongoing all-sky experiment *Planck* (The Planck Collaboration 2006). We consider the range of harmonics (2, 2000). However, the results presented here are also applicable to smaller surveys such as Arcminute Cosmology Bolometer Array Receiver (ACBAR;[4] Runyan et al. 2003) which covers the ℓ-range (2000, 3000). ACBAR is a multifrequency millimetre-wave receiver designed for observations of the CMB and the SZ effect. The ACBAR focal plane consists of a 16 pixel, background-limited, 240 mK bolometer array that can be configured to observe simultaneously at 150, 220, 280 and

[4] http://cosmology.berkeley.edu/group/swlh/acbar/

350 GHz with 4–5 arcmin full width at half-maximum (FWHM). Together with *Planck* these two experiments cover the entire range of ℓ values up to 3000. In addition to *Planck* we also consider a noise-free ideal set-up for the range of ℓ values (2, 2000) as a reference.

The paper is organized as follows. In Section 2, we review the details of the analytical models involving the power spectrum and the bispectrum of the tSZ effect. In Section 3, we present the skewness parameters that can be used to study the MFs. In Section 4, we define the triplets of generalized MFs, we propose the use of skew-spectra associated with individual generalized skewness parameters that carry more information than the ordinary MFs and we show how these skew-spectra are associated with the MFs and are related to the generalized skewness parameters. Next, in Section 5, we present estimators that can be used to extract the skew-spectra from a noisy data set in the presence of an observational mask and arbitrary beam. We also obtain the signal-to-noise ratio (S/N) for these skew-spectra for realistic observational scenarios. Finally, Section 6 is devoted to a discussion of our results and future prospects.

The particular cosmology that we adopt for numerical study is specified by the following parameter values (to be introduced later): $\Omega_\Lambda = 0.741,\ h = 0.72,\ \Omega_{\rm b} = 0.044,\ \Omega_{\rm CDM} = 0.215,\ \Omega_{\rm M} = \Omega_{\rm b} + \Omega_{\rm CDM},\ n_{\rm s} = 0.964,\ w_0 = -1,\ w_{\rm a} = 0,\ \sigma_8 = 0.803$ and $\Omega_\nu = 0$.

2 LOWER ORDER STATISTICS OF THE tSZ EFFECT

In this section, we briefly review the two different approaches that are commonly used to model the tSZ effect (for more details see Cooray, Baumann & Sigurdson 2005, and the references therein). We use these models to study the morphological properties of the SZ effect. The tSZ temperature fluctuation $\Theta^{\rm SZ}(\hat{\Omega}, \nu) = \delta T(\hat{\Omega}, \nu)/T_{\rm CMB}$ is given by the (opacity-weighted) pressure fluctuation, i.e.

$$\delta T(\hat{\Omega})/T_{\rm CMB} \equiv g_\nu(x) y(\hat{\Omega}) = g_\nu(x) \int_0^{\eta_0} {\rm d}\eta\ a(\eta)\ \sigma_{\rm T}/m_{\rm e}\ \pi_{\rm e}(\hat{\Omega}, \eta), \tag{1}$$

we will use the symbol η_0 to represent the conformal distance to the surface of last scattering. The electron pressure is denoted as $\pi_{\rm e} = n_{\rm e} k_{\rm B} T_{\rm e}$. Here $y(\hat{\Omega})$ is the Compton y-parameter, $\sigma_{\rm T}$ is the Thomson cross-section, $k_{\rm B}$ is the Boltzmann constant, $m_{\rm e}$ is the electron rest mass, $n_{\rm e}$ is the electron number density and $T_{\rm e}$ the electron temperature. The function $g_\nu(x)$ encodes the frequency dependence of the tSZ anisotropies. It relates the temperature fluctuations at a frequency ν with the Compton parameter y, i.e. $g_\nu(x) = x\coth(x/2) - 4$ and $x = (h\nu/k_{\rm B}T_{\rm CMB}) = \nu/(56.84\,{\rm GHz})$. In the low-frequency part of the spectrum $g_\nu(x) = -2$, for $x \ll 1$, here x is the dimensionless frequency as defined above. Unless stated otherwise all our results will be for the low-frequency limiting case. The conformal time η can be expressed in terms of the cosmological density parameters $\Omega_{\rm M}$, $\Omega_{\rm K}$ and Ω_Λ by the following expression: $\eta(z) = \int_0^z {\rm d}z'/H(z')$ and $E^2(z) = H^2(z)/H_0^2 = [\Omega_{\rm M}(1+z)^3 + \Omega_{\rm K}(1+z)^2 + \Omega_\Lambda]$. Introducing the τ the Thompson optical depth and the fractional fluctuations in pressure as $\delta\pi = \delta p_{\rm e}/p_{\rm e}$ we can write $\Theta^{\rm SZ}(\hat{\Omega}, \nu) = g_\nu(x) \int_0^{r_0} {\rm d}r\ \dot{\tau}\pi(\hat{\Omega}; r)$. Here r is the comoving distance, r_0 is the distance to the last scattering surface, τ is the Thomson optical depth and overdot represents derivatives with respect to r.

We will primarily be working in the Fourier domain. The three-dimensional (3D) electron pressure π can be decomposed into its Fourier coefficients using the following convention that we will follow: $\delta\pi(\boldsymbol{k}) = \int {\rm d}^3\boldsymbol{x}\ \delta\pi(\boldsymbol{x}) \exp[-{\rm i}\boldsymbol{k}\cdot\boldsymbol{x}]$. The projected statistics that we will consider can be related to the 3D statistics which are defined by the following expressions which specify the power spectrum $P_\pi(k; r)$, the bispectrum $B_\pi(k_1, k_2, k_3; r)$ and the trispectrum $T_\pi(k_1, k_2, k_3, k_4; r)$ in terms of the Fourier coefficients (throughout we will use a semicolon to separate the temporal arguments r_i from other variables that specify a multispectra):

$$\langle \delta\pi(\boldsymbol{k}_1; r_1)\delta\pi(\boldsymbol{k}_2; r_2)\rangle_{\rm c} = (2\pi)^3 P_\pi(k_1; r_1, r_2)\delta_{\rm 3D}(\boldsymbol{k}_1 + \boldsymbol{k}_2), \tag{2}$$

$$\langle \delta\pi(\boldsymbol{k}_1; r_1)\delta\pi(\boldsymbol{k}_2; r_2)\delta\pi(\boldsymbol{k}_3; r_3)\rangle_{\rm c} = (2\pi)^3 B_\pi(k_1, k_2, k_3; r_i)\delta_{\rm 3D}(\boldsymbol{k}_1 + \boldsymbol{k}_2 + \boldsymbol{k}_3), \tag{3}$$

$$\langle \delta\pi(\boldsymbol{k}_1; r_1)\delta\pi(\boldsymbol{k}_2; r_2)\delta\pi(\boldsymbol{k}_3; r_3)\delta\pi(\boldsymbol{k}_4; r_4)\rangle_{\rm c} = (2\pi)^3 T_\pi(k_1, k_2, k_3, k_4; r_i)\delta_{\rm 3D}(\boldsymbol{k}_1 + \boldsymbol{k}_2 + \boldsymbol{k}_3 + \boldsymbol{k}_4). \tag{4}$$

Our aim is to relate the statistics of pressure fluctuations $\delta\pi(\boldsymbol{x})$ to those of the underlying density fluctuations $\delta(\boldsymbol{x})$. The hierarchy of higher order correlation functions can be defined using a similar set of equations. The corresponding multispectra will be denoted with a subscript δ, i.e. B_δ and T_δ will represent the bi- and trispectrum of the underlying density contrast, and the power spectrum will be denoted as P_δ. The $\delta_{\rm 3D}$ functions represent the 3D Dirac delta function, and represent translational invariance of corresponding correlation hierarchy in real space. The unequal time correlators appearing in the expressions of the multispectra will typically collapse to equal time correlators due to the use of Limber approximations that we discuss next.

2.1 Linking projected statistics with 3D statistics

The spherical harmonics decomposition of the projected field $\Theta^{\rm SZ}(\hat{\Omega})$ will be represented as $\Theta^{\rm SZ}_{lm}$ can be expressed in terms of a weight $W^{\rm SZ}(r)$. We will henceforth suppress the frequency ν dependence of $a^{\rm SZ}_{lm}$ as well as $\Theta^{\rm SZ}(\hat{\Omega})$. The line-of-sight integration over r projects the 3D $\delta_{lm}(\boldsymbol{k}; r)$ on to the harmonics $a^{\rm SZ}_{lm}$:

$$\Theta^{\rm SZ}_{lm} = (2\pi)^{-3/2} \int {\rm d}\hat{\Omega}\ Y^*_{lm}(\hat{\Omega})\ \Theta^{\rm SZ}(\hat{\Omega}) = \sqrt{\frac{2}{\pi}} \int_0^{r_0} {\rm d}r\ W^{\rm SZ}(r) \int k^2{\rm d}k \int {\rm d}\Omega_{\rm k}\ i^l\ j_l(kr) Y^*_{lm}(\hat{\Omega}_{\rm k})\delta(\boldsymbol{k}; r),$$
$$W^{\rm SZ}(r) = -2b_\pi(r)\dot{\tau}; \quad \dot{\tau} = ca\sigma_{\rm T} n_{\rm e}(z). \tag{5}$$

Here $Y_{lm}(\hat{\Omega})$ represents a spherical harmonic and $j_l(kr)$ is the spherical Bessel function of order l. The weight $W^{\rm SZ}(r)$ is introduced by projecting the 3D statistics on to the sky. We use the following relation to relate $\delta_{lm}(\boldsymbol{k}; r)$ in the spherical basis with $\delta(\boldsymbol{k}; r)$ in Fourier basis to

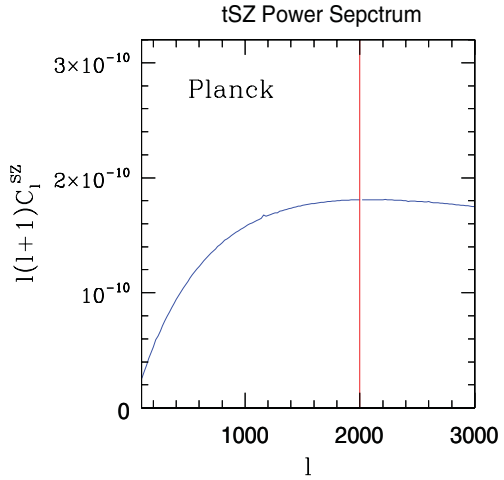

Figure 1. The power spectrum of SZ is depicted for our choice of cosmological parameters. The halo model was used for the computation of the power spectrum. See Section 2.3 for a short discussion and relevant parameter values. For an all-sky *Planck*-type experiment we consider the range $l = (2, 2000)$.

obtain

$$\delta_{lm}(\boldsymbol{k}; r) = (2\pi)^{-3/2} \int \mathrm{d}\hat{\Omega}_\mathrm{k}\; Y_{lm}(\hat{\Omega}_\mathrm{k})\; \delta(\boldsymbol{k}; r). \tag{6}$$

Here Ω_k specifies angular direction in the Fourier domain as opposed to Ω which describes angular position in the sky. We can use this expression next in equation (5) and use the definition of power spectrum from equation (2). Using the integral representation of the Dirac's delta function $\delta_{3\mathrm{D}}(\boldsymbol{k}) = (2\pi)^{-3} \int \exp(\mathrm{i}\boldsymbol{k}\cdot\boldsymbol{x})\mathrm{d}^3\boldsymbol{x}$; in association with the Rayleigh's expansion of the plane wave in terms of spherical harmonics $\exp(\mathrm{i}\boldsymbol{k}\cdot\boldsymbol{x}) = 4\pi\sum_{lm} i^l\, j_l(kx) Y_{lm}(\hat{\Omega}_\mathrm{k}) Y_{lm}(\hat{\Omega})$. Using these expression we arrive at the following expression which projects the 3D power spectrum $P_\pi(k; r_1, r_2)$ to the spherical sky (Cooray 2001b):

$$\mathcal{C}_l^{\mathrm{SZ}} = \frac{2}{\pi} \int W^{\mathrm{SZ}}(r_1)\mathrm{d}r_1 \int W^{\mathrm{SZ}}(r_2)\mathrm{d}r_2 \int \mathrm{d}k\, k^2\, j_{l_1}(kr_1)\, j_{l_2}(kr_2) P_\pi(k; r_1, r_2). \tag{7}$$

The following form of Limber's approximation (Limber 1954; LoVerde & Afshordi 2008) is remarkably accurate at small angular scales; i.e. for $l \geq 100$ we have $\int \mathrm{d}k\, k^2\, F(k)\, j_l(kr_1) j_l(kr_2) = (\pi/2r_1^2) F(l/r_1)\delta_\mathrm{D}(r_1 - r_2)$. The use of this form of Limber's approximation greatly simplifies the subsequent results by reducing the correlators of multiple time slices to single-time correlators (Cooray 2001b):

$$\mathcal{C}_l^{\mathrm{SZ}} = \left\langle \Theta_{lm}^{\mathrm{SZ}} \Theta_{lm}^{\mathrm{SZ}*} \right\rangle = \int_0^{r_0} \mathrm{d}r\, \frac{[W^{\mathrm{SZ}}(r)]^2}{d_\mathrm{A}^2(r)} P_\pi\left(\frac{l}{d_\mathrm{A}(r)}; r\right). \tag{8}$$

Here $d_\mathrm{A}(r)$ is the angular diameter distance in terms of the comoving radial distance r. The power spectrum $\mathcal{C}_l^{\mathrm{SZ}}$ is plotted in Fig. 1 as a function of the harmonics l.

The bispectrum in the harmonic domain is represented by the following three-point correlation function:

$$B_{l_1 l_2 l_3}^{\mathrm{SZ}} \equiv \sum_{m_1 m_2 m_3} \begin{pmatrix} l_1 & l_2 & l_3 \\ m_1 & m_2 & m_3 \end{pmatrix} \left\langle \Theta_{l_1 m_1}^{\mathrm{SZ}} \Theta_{l_2 m_2}^{\mathrm{SZ}} \Theta_{l_3 m_3}^{\mathrm{SZ}} \right\rangle_\mathrm{c}. \tag{9}$$

The matrix above in equation (9) represents the Wigner 3*j* symbols (Edmonds 1968) and $B_{l_1 l_2 l_3}^{\mathrm{SZ}}$ defines the tSZ bispectrum in the spherical sky. The equation linking the projected bispectrum $B_{l_1 l_2 l_3}^{\mathrm{SZ}}$ and its 3D analogue $B_\pi(k_1, k_2, k_3)$, defined in equation (3), can be derived following exactly the same procedure. We quote here the final expression which takes the following form (Cooray 2001b):

$$B_{l_1 l_2 l_3}^{\mathrm{SZ}} = I_{l_1 l_2 l_3} \int \mathrm{d}r\, \frac{[W^{\mathrm{SZ}}(r)]^3}{d_\mathrm{A}^3(r)} B_\pi\left(\frac{l_1}{d_\mathrm{A}(r)}\frac{l_2}{d_\mathrm{A}(r)}\frac{l_3}{d_\mathrm{A}(r)}; r\right), \quad I_{l_1 l_2 l_3} = \sqrt{\frac{(2l_1+1)(2l_2+1)(2l_3+1)}{4\pi}}. \tag{10}$$

Next we describe models for the 3D power spectrum $P_\pi(k; r)$ and bispectrum $B_\pi(k_1, k_2, k_3; r)$ that are used for computation of the projected SZ versions $\mathcal{C}_l^{\mathrm{SZ}}$ and $B_{l_1 l_2 l_3}^{\mathrm{SZ}}$. Modelling of the tSZ statistics requires a model for the clustering of the underlying dark matter distribution δ. We will employ extensions of perturbative calculations as well as halo model predictions to model the underlying statistics of dark matter clustering. We describe these models in following subsections. We have shown the angular power spectrum $\mathcal{C}_l^{\mathrm{SZ}}$ for the SZ effect in Fig. 1 as a function of harmonic number l. For the computation of this power spectrum a halo model approach was used to be discussed in Section 2.3. As we discussed in the Introduction, modelling the tSZ statistics involves modelling of the underlying dark matter clustering along with its relationship with the baryonic clustering and hence the fluctuation in baryonic pressure. This modelling has so far been performed using two complimentary approaches. In the simpler approach, the clustering of dark matter is described using second-order perturbation theory or its extensions. The clustering of baryons is described using a biasing scheme. These inputs are sufficiently accurate to model the SZ sky, in particular at larger length-scales. We will consider the linear biasing model first.

2.2 Linear biasing and perturbative approach

In a perturbative approach, gravitational dynamics is analysed by expanding the large-scale density field δ in a perturbative series; a redshift-dependent linear biasing is assumed (Goldberg & Spergel 1999a,b). This is all valid as long as the variance of the density contrast is smaller than unity, and such a treatment is suitable for the diffuse tSZ component (Hansen et al. 2005). For large smoothing scales such calculations can provide valuable insights to gravitational dynamics. The perturbative bispectrum $B_\delta(k_1, k_2, k_3; r)$ for the density contrast δ from such calculations is given by (Peebles 1971; Fry 1984; Bouchet et al. 1992)

$$B_\delta(k_1, k_2, k_3; r) = F_2(k_1, k_2)P_\delta(k_1; r)P_\delta(k_2; r) + \text{cyc.perm.}, \tag{11}$$

$$F_2(k_1, k_2) = 1 - \frac{2}{7}\Omega_{\rm M}^{-2/63} + \frac{\boldsymbol{k}_1 \cdot \boldsymbol{k}_2}{2k_1k_2}\left(\frac{k_1}{k_2} + \frac{k_2}{k_1}\right) + \frac{2}{7}\Omega_{\rm M}^{-2/63}\frac{(\boldsymbol{k}_1 \cdot \boldsymbol{k}_2)^2}{k_1^2k_2^2}. \tag{12}$$

In the deeply non-linear regime we do not have a complete analytical model of gravitational clustering. Typically, plausible approximations that include the halo model (to be discussed next) are used for this purpose, with varying degree of success. One such ansatz is the well known *hierarchical ansatz* that assumes the higher order correlation functions can be constructed from the products of two-point correlation functions (Bernardeau et al. 2002). The different tree diagrams thus constructed are all represented by various *hierarchical amplitudes* which are left arbitrary. The bispectrum in such a hierarchical scenario takes the following form:

$$B_\delta(k_1, k_2, k_3; r) = Q_3(n)[P_\delta(k_1; r)P_\delta(k_2; r) + \text{cyc.perm.}], \quad Q_3(n) = [4 - 2^n]/[1 + 2^{n+1}]. \tag{13}$$

The expression for $Q_3(n)$ is adopted from Scoccimarro & Frieman (1999), here n is the local linear power spectral index. For a generic power spectrum one can replace n with the local linear power spectral index at $(k_1 + k_2 + k_3)/3$ (Hui 1999). More elaborate schemes that interpolate the quasi-linear regime and the highly non-linear regime have been devised in recent years (Scoccimarro & Couchman 2001). Though we restrict ourselves to the computation of the bispectrum in this paper, the approach can also be extended beyond third order. The hierarchical ansatz captures the salient features of non-linear clustering; the expressions are relatively simpler than the full perturbative expressions and have been tested in a variety of cosmological contexts. In connecting the statistics of the electron pressure field π, namely the power spectrum $P_\pi(k; r)$ and $B_\pi(k_1, k_2, k_3; r)$, we will use the following local biasing model $P_\pi(k; r) = b_\pi(r)^2P_\delta(k; r)$ and $B_\pi(k_1, k_2, k_3; r) = b_\pi(r)^3B_\delta(k_1, k_2, k_3; r)$. Following Goldberg & Spergel (1999a,b) and Cooray (2000, 2001b), the bias is chosen to be of the form $b_\pi(r) = b_\pi(0)/(1 + z)$ with $b_\pi(0) = k_{\rm B}T_{\rm e}(0)/(m_{\rm e}c^2b_\delta)$. In our calculation, we take $b_\pi(r) = 0.0039/(1 + z)$. These 3D Fourier statistics are the ingredients for the computation of the projected statistics on the surface of the sky using equations (8) and (10).

2.3 Halo model and tSZ: a brief review

The halo model description of large-scale structure relies on modelling of the clustering of haloes and predictions from perturbative calculations to model the non-linear correlation functions. In the context of the halo model, the dark matter is assumed to be in collapsed haloes that are characterized by their mass, radial profile, halo occupation numbers and underlying correlation hierarchy. The baryonic fluid is assumed to be in equilibrium with the dark matter profile, and is characterized by a specific equation of state. The use of the halo model is well established in cosmology and has a long history (Cooray & Seth 2002). It has been used relatively recently in modelling of clustering of galaxies, weak lensing observables and statistics of CMB secondaries. In the context of tSZ, it has been used to compute the leading order non-Gaussianity such as the bispectrum, as well as higher order statistics such as the trispectrum, which is important in computing the covariance of the ordinary power spectrum. It is known that the halo overdensity at a given position $\boldsymbol{x}$, $\delta^{\rm h}(\boldsymbol{x}, M; z)$ can be related to the underlying density contrast $\delta(\boldsymbol{x}; z)$ by a Taylor expansion, as was shown by (Mo & White 1996)

$$\delta^{\rm h}(\boldsymbol{x}, M; z) = \left[b_1(M; z)\delta(\boldsymbol{x}; z) + \frac{1}{2}b_2(M; z)\delta^2(\boldsymbol{x}; z) + \cdots\right]. \tag{14}$$

The expansion coefficients are functions of the threshold $\nu(M; z) = \delta_{\rm c}(z)/\sigma(M; z)$, where $\delta_{\rm c}$ is the threshold for a spherical overdensity to collapse, and $\sigma(M; z)$ is the rms fluctuation within a top-hat filter. The parameter $\delta_{\rm c}(z)$ is the value of the spherical overdensity at which it collapses at a redshift z and is given by the following functional fit for a given Ω_Λ and $\Omega_{\rm M}$:

$$\delta_{\rm c}(z) = \frac{3(12\pi)^{2/3}}{20}\left[1 - \frac{5}{936}\ln\left(1 + \frac{1 - \Omega_{\rm M}}{\Omega_{\rm M}(1 + z)^3}\right)\right]. \tag{15}$$

The rms fluctuation in the sphere of radius R is constructed from the linearly extrapolated power spectrum $P(k; r)$: $\sigma^2(M; z) = D^2(z)\int {\rm d}\ln k\Delta^2(k; z)|W(kR)|^2$, where $W(x)$ is the top-hat window, and $\Delta^2(k)$ is the dimensionless power spectrum as given by $\Delta^2(k; z) = k^3P(k; z)/2\pi^2$. The linear order bias $b_1(M; z)$ introduced in this expansion of $\delta_{\rm h}$ in terms of underlying density contrast δ depends on the threshold $\nu(M; z)$ (Mo, Jing & White 1997):

$$b_1(M; z) = 1 + \frac{(a\nu^2(M; z) - 1)}{\delta_{\rm c}(z)} + \frac{2p}{\delta_{\rm c}(z)\{1 + [a\nu^2(M; z)]^p\}}. \tag{16}$$

The linear growth factor $D(z)$ is defined by the following expression: $D(z) \propto H(z)\int_z^\infty {\rm d}z'(1 + z')[H(z')]^{-3}$ and is normalized to unity at $z = 0$, i.e. $D(0) = 1$. The two main ingredients in the halo model are the radial profile of the haloes and the number density of haloes. The number density is given by $f(\nu) = \sqrt{2A^2a^2/\pi}[1 + (a\nu^2)^{-p}]\exp(-a\nu^2/2)$ for the threshold ν. The parameters (p, a) take the value (0, 1) for the Press–Schechter mass function (Press & Schechter 1974). The constant A is determined by imposing the normalization $\int f(\nu)\,{\rm d}\nu = 1$. The

halo model incorporates perturbative aspects of gravitational dynamics through the halo–halo correlation hierarchy. The non-linear features take direct contribution from the halo profile; the number density of haloes also needs to be determined. The total power spectrum $P^{\rm t}(k;z)$ at non-linear scale can be written as the sum of two separate contributions to the power spectrum: $P^{\rm t}_{\pi}(k;z) = P^{\rm 1h}{}_{\pi}(k;z) + P^{\rm 2h}_{\pi}(k;z)$ (Seljak 2000). These represent the contribution from clustering of dark matter particles in two different haloes, i.e. the halo–halo term $P^{\rm 2h}$, and the contribution from a single halo, i.e. one-halo term $P^{\rm 1h}$. These terms are in turn expressed in terms of two integrals:

$$P^{\rm 1h}_{\pi}(k;z) = I^{0}_{2,\pi}(k;z), \quad P^{\rm 2h}_{\pi}(k;z) = \left[I^{(0)}_{1,\pi}(k;z)\right]^2 P_{\delta}(k;z). \tag{17}$$

The integrals themselves depend on the number counts of haloes as a function of the concentration parameter c and the mass M:

$$I^{(0)}_{2,\pi}(k;z) = \int {\rm d}M \int {\rm d}c \frac{{\rm d}^2 n}{{\rm d}M\,{\rm d}c} \,|\,\pi_{\rm e}(k|M,c;z)|^2, \quad I^{(1)}_{1,\pi}(k;z) = \int {\rm d}M \int {\rm d}c \frac{{\rm d}^2 n}{{\rm d}M\,{\rm d}c} b_1(M;z)\,|\,\pi_{\rm e}(k\,|\,M,c;z)|. \tag{18}$$

The bispectrum can be expressed in an analogous manner:

$$B^{\rm t}_{\pi}(k_1,k_2,k_3;z) = B^{\rm 3h}_{\pi}(k_1,k_2,k_3;z) + B^{\rm 2h}_{\pi}(k_1,k_2,k_3;z) + B^{\rm 1h}_{\pi}(k_1,k_2,k_3;z), \tag{19}$$

$$B^{\rm 1h}_{\pi} = I^{0}_{3}(k_1,k_2,k_3;z), \quad B^{\rm 2h}_{\pi}(k_1,k_2,k_3;z) = I^{1}_{2}(k_1,k_2;z) I^{0}_{1}(k_3;z) P_{\pi}(k_3;z) + {\rm cyc.perm.}, \tag{20}$$

$$B^{\rm 3h}_{\pi} = \left[2J(k_1,k_2,k_3;z) I^{1}_{1}(k_3;z) + I^{2}_{1}(k_3;z)\right] I_1(k_1;z) I_1(k_2;z) P_{\pi}(k_1;z) P_{\pi}(k_2;z) + {\rm cyc.perm.} \tag{21}$$

The kernel $J(k_1,k_2,k_3;z)$ is same as $F_2(k_1,k_2,k_3;z)$ introduced in equation (12). We have introduced the following notation above:

$$I^{(p)}_{q,\pi}(k;z) = \int {\rm d}M \int {\rm d}c \frac{{\rm d}^2 n}{{\rm d}M\,{\rm d}c} b_p(M;z)\,|\,\pi_{\rm e}(k\,|\,M,c;z)|^q. \tag{22}$$

The Fourier transform of the halo electron pressure profile $\pi(r)$ is denoted by $\pi_{\rm e}(k)$ above:

$$\pi_{\rm e}(k) = \int {\rm d}^3\boldsymbol{r}\, \pi_{\rm e}(r)\, \exp(-{\rm i}\boldsymbol{k}\cdot\boldsymbol{r}) = \int_0^{\infty} 4\pi r^2\, {\rm d}r\, \pi_{\rm e}(r) \frac{\sin(kr)}{kr}. \tag{23}$$

For the dark matter profile we assume $\rho_{\rm d}(r) \equiv \rho_{\rm s} u^{-1}(1+u)^{-2}$ with $u \equiv r/r_{\rm s}$. Here the dark matter is assumed to follow an NFW profile, and $r_{\rm s}$ is the characteristic scale radius. In the context of the spherical collapse model, the outer extent of a cluster is taken to be its virial radius $r_{\rm v} = [3M/4\pi\rho_{\rm M}(z)\Delta(z)]$, where $\rho_{\rm M}(z)$ is the mean background matter density of the universe at redshift z, and $\Delta_{\rm M}(z)$ is the overdensity of the halo relative to the background density. The ratio of the virial radius to the scale radius is called the concentration parameter $c \equiv r_{\rm v}/r_{\rm s}$. Together, c and M determine the dark matter distribution of a given halo. The gas density profile in terms of the dimensionless parameter u is $\rho_{\rm g}(u) \equiv \rho_0 \rho_{\rm g}(u)$. In this particular case a polytropic equation of state is typically used. According to numerical simulations, clusters of a given mass have a range of concentration parameters. The number density of clusters with a given mass M and concentration parameter c is expressed in terms of a bivariate distribution function ${\rm d}^2 n(M,c;z)/{\rm d}M\,{\rm d}c = {\rm d}n/{\rm d}M(M;z) P(c\,|\,M;z)$. The conditional probability distribution function of a halo having concentration c for a given mass M in numerical simulations was found to be well approximated by a lognormal distribution. $P(c\,|\,M;z){\rm d}c = \exp[-(\log c - \log \bar{c})/2\sigma_{\log c}]{\rm d}c/(c\ln(10))$ with $\bar{c}(M,z) = c_0/1 + z\,[M/M_{\star}(z=0)]^{-\alpha_c}$. Here $M_{\star}$ is the mass scale at which $\nu(M_{\star};z) = 1$, $c_0 = 9$, $\alpha_c = 0.13$ and $\sigma_{\log c} = 0.14$. More complicated models are possible where a mass-dependent $\sigma_{\log c}$ can be incorporated. For a lengthier discussion of the equilibrium baryonic gas profile and its relation to the underlying halo profile, see Cooray et al. (2005). We have considered the halo mass range 10^{11}–$10^{16}\,{\rm M}_{\odot}$ in our calculations.

3 MINKOWSKI FUNCTIONALS

In this section we will review the basics of the MFs in brief. The MFs are morphological descriptors well known in cosmology. Put simply, morphological properties are the properties that remain invariant under rotation and translation; see e.g. Hadwiger (1959) for a more mathematical discussion. We will concentrate on a set of three MFs defined in 2D that are defined over an excursion set Σ with a boundary $\partial\Sigma$ for a given threshold ν. Following the notation of Hikage et al. (2008) we define

$$V_0(\nu) = \int_{\Sigma} {\rm d}a, \quad V_1(\nu) = \frac{1}{4}\int_{\partial\Sigma} {\rm d}l, \quad V_2(\nu) = \frac{1}{2\pi}\int_{\partial\Sigma} \mathcal{K}{\rm d}l. \tag{24}$$

Here $\mathcal{K}$ denotes the curvature along the boundary $\partial\Sigma$. The three MFs $V_0(\nu)$, $V_1(\nu)$ and $V_2(\nu)$ correspond to the area of the excursion set Σ, the length of its boundary $\partial\Sigma$ as well as the integral of curvature $\mathcal{K}$ along its boundary which is also related to the genus and hence the Euler characteristics. The MFs can be decomposed into two different contributions: Gaussian $V^{\rm G}_k(\nu)$ and non-Gaussian $\delta V_k(\nu)$, i.e. $V_k(\nu) = V^{\rm G}_k(\nu) + \delta V_k(\nu)$ with $\nu = \Theta/\sigma_0$ and $\sigma_0^2 = \langle\Theta^2\rangle$. We will further separate out an amplitude A in the expressions of both of these contributions which depend only on the power spectrum of the perturbation through σ_0 and σ_1 (see e.g. Hikage et al. 2008):

$$V^{\rm G}_k(\nu) = A\exp\left(-\frac{\nu^2}{2}\right) H_{k-1}, \qquad \delta V_k(\nu) = A\exp\left(-\frac{\nu^2}{2}\right)\left[\delta V^{(2)}_k(\nu)\sigma_0 + \delta V^{(3)}_k(\nu)\sigma_0^2 + \delta V^{(4)}_k(\nu)\sigma_0^3 + \cdots\right], \tag{25}$$

$$\delta V^{(2)}_k(\nu) = \left[\left\{\frac{1}{6}S^{(0)}H_{k+2}(\nu) + \frac{k}{3}S^{(1)}H_k(\nu) + \frac{k(k-1)}{6}S^{(2)}H_{k-2}(\nu)\right\}\right], \qquad A = \frac{1}{(2\pi)^{(k+1)/2}}\frac{\omega_2}{\omega_{2-k}\omega_k}\left(\frac{\sigma_1}{\sqrt{2}\sigma_0}\right)^k. \tag{26}$$

The constant ω_k introduced above is the volume of the unit sphere in k dimensions: $\omega_k = \pi^{k/2}/\Gamma(k/2+1)$ in 2D where we will only need $\omega_0 = 1$, $\omega_1 = 2$ and $\omega_2 = \pi$. The Hermite polynomials $H_k(\nu)$ appear in the expression for MFs for a weakly non-Gaussian random field.

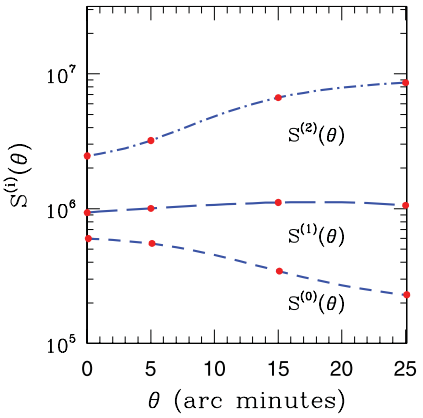

Figure 2. The three one-point skewness parameters $S^{(0)}$ (short-dashed), $S^{(1)}$ (long-dashed) and $S^{(2)}$ (dot–dashed) are plotted as a functions of the FWHM θ for a Gaussian beam. The results plotted are for ideal surveys without instrumental noise. The skewness parameter $S^{(0)}$ is the ordinary skewness describing the departure from non-Gaussianity at the lowest order. The points are results from numerical computations using the halo model, and the lines denote smooth fits to the results. The one-point skewness parameters $S^{(i)}$ is related to the skew-spectra $S_l^{(i)}$ through the following expression: $S^{(i)} = \sum_l (2l+1) S_l^{(i)}$.

The lowest order departure from Gaussianity $\delta V_k^{(2)}(\nu)$ is encoded in three different generalized skewness parameters: $S^{(0)}, S^{(1)}$ and $S^{(2)}$. The next-to-leading order correction terms $\delta V_k^{(2)}(\nu)$ are typically neglected as they are an order of magnitude smaller. Just as the generalized (three) skewness parameters they can be constructed from the generalization of kurtosis. All three skewness parameters can be constructed from the bispectrum using different weights to sample different modes. In our next section, we discuss these generalized skewness parameters and introduce the power spectra associated with them. We denote the power spectra with $S_l^{(0)}, S_l^{(1)}$ and $S_l^{(2)}$. These carry more information than their one-point counterparts of the generalized skewness parameters.

Estimation of MFs typically is done directly by employing a grid-based approach in real space, so that the integrals introduced in equation (24) are estimated on a discrete set of points. Here we will show that the computation of $S_l^{(i)}$ introduced in equation (26) can also be done in harmonic space. This will be particularly suitable for near all-sky surveys where galactic masks and point source masks can be incorporated in the analysis relatively easily. This will allow a cross-comparison of both methods for any systematics as well as residuals from component separation. We will deal with near all-sky surveys, but flat-sky results can also be recovered using standard procedure, which will be suitable for smaller patch-sky surveys.

Fig. 2 shows the parameters $S^{(0)}$, $S^{(1)}$ and $S^{(2)}$ as a function of FWHM assuming a Gaussian beam. We have assumed a halo model for computation of these generalized skewness parameters. The parameters defined in equation (26), σ_0 and σ_1, appear in the perturbative expansion of the MFs as well as in their normalization. These parameters depend on the level of noise.

4 GENERALIZED SKEW-SPECTRA AND MFS

The skew-spectra are cubic statistics that are constructed by cross-correlating two different fields. One of the fields used is a composite field, typically a product of two maps either in original form or constructed by means of relevant differential operations. The second field will typically be a single field, but may be constructed by using differential operators on the original field. All of these three skewness contribute to the three MFs that we will consider in 2D. The first skew-spectrum was studied by Cooray (2001a), later generalized by Munshi & Heavens (2010), and is related to commonly used skewness. The skewness in this case is constructed by cross-correlating the squared map $[\Theta^2(\hat{\Omega})]$ with the original map $[\Theta(\hat{\Omega})]$. The second skew-spectrum is constructed by cross-correlating the squared map $[\Theta^2(\hat{\Omega})]$ against $[\nabla^2\Theta(\hat{\Omega})]$. Analogously the third skew-spectrum represents the cross-spectra that can be constructed using $[\nabla\Theta(\hat{\Omega})\cdot\nabla\Theta(\hat{\Omega})]$ and $[\nabla^2\Theta(\hat{\Omega})]$ maps which are derived in equations (34)–(36):

$$S_l^{(0)} \equiv \frac{1}{12\pi\sigma_0^4} S_l^{(\Theta^2,\Theta)} \equiv \frac{1}{12\pi\sigma_0^4}\frac{1}{2l+1}\sum_m \mathrm{Real}([\Theta]_{lm}[\Theta^2]^*_{lm}) = \frac{1}{12\pi\sigma_0^4}\sum_{l_1 l_2}\mathcal{B}_{l l_1 l_2} J_{l l_1 l_2} W_l W_{l_1} W_{l_2}, \tag{27}$$

$$S_l^{(1)} \equiv \frac{1}{16\pi\sigma_0^2\sigma_1^2} S_l^{(\Theta^2,\nabla^2\Theta)} \equiv \frac{1}{16\pi\sigma_0^2\sigma_1^2}\frac{1}{2l+1}\sum_m \mathrm{Real}([\nabla^2\Theta]_{lm}[\Theta^2]^*_{lm}) \tag{28}$$

$$= \frac{1}{16\pi\sigma_0^2\sigma_1^2}\sum_{l_i}[l(l+1)+l_1(l_1+1)+l_2(l_2+1)]\mathcal{B}_{l l_1 l_2} J_{l l_1 l_2} W_l W_{l_1} W_{l_2}, \tag{29}$$

$$S_l^{(2)} \equiv \frac{1}{8\pi\sigma_1^4} S_l^{(\nabla\Theta\cdot\nabla\Theta,\nabla^2\Theta)} \equiv \frac{1}{8\pi\sigma_1^4}\frac{1}{2l+1}\sum_m \mathrm{Real}([\nabla\Theta\cdot\nabla\Theta]_{lm}[\nabla^2\Theta]^*_{lm})$$

$$= \frac{1}{8\pi\sigma_1^4}\sum_{l_i}[[l(l+1)+l_1(l_1+1)-l_2(l_2+1)]l_2(l_2+1)+\mathrm{cyc.perm.}]\mathcal{B}_{l l_1 l_2} J_{l l_1 l_2} W_l W_{l_1} W_{l_2}, \tag{30}$$

$$J_{l_1 l_2 l_3} \equiv \frac{I_{l_1 l_2 l_3}}{2l_3+1} = \sqrt{\frac{(2l_1+1)(2l_2+1)}{(2l_3+1)4\pi}} \begin{pmatrix} l_1 & l_2 & l_3 \\ 0 & 0 & 0 \end{pmatrix}, \tag{31}$$

$$S^{(i)} = \sum_l (2l+1) S_l^{(i)}, \tag{32}$$

$$\sigma_j^2 = \frac{1}{4\pi} \sum_l (2l+1)[l(l+1)]^j \mathcal{C}_l W_l^2. \tag{33}$$

This set of equations constitutes one of the main results of this paper. The matrices here denote the Wigner 3*j* symbols (Edmonds 1968), W_l represents the smoothing window which can be e.g. top-hat or Gaussian or compensated. Each of these spectra probes the same bispectrum $B_{ll_1l_2}$ but with different weights for individual triplets of modes (l, $l_1 l_2$), specifying a triangle in the harmonic domain. The skew-spectrum sums over all possible configurations of the bispectrum keeping one of its side l fixed. For each individual choice of l we can compute the skew-spectra $S_l^{(i)}$. The extraction of skew-spectra from data is relatively straightforward. It consists of construction of the relevant maps in real space either by algebraic or differential operation and then cross-correlating them in the multipole domain. Issues related to mask and noise will be dealt with in later sections. We will show that even in the presence of mask the computed skew-spectra can be inverted to give an unbiased estimate of all-sky skew-spectra. Presence of noise will only affect the scatter. We have explicitly displayed the experimental beam b_l in all of our expressions.

To derive the above expressions, we first express the spherical harmonic expansion of fields $[\nabla^2\Theta(\hat{\Omega})]$, $[\nabla\Theta(\hat{\Omega})\cdot\nabla\Theta(\hat{\Omega})]$ and $[\Theta^2(\hat{\Omega})]$ in terms of the harmonics of the original fields Θ_{lm}. These expressions involve the 3*j* functions as well as factors that depend on various l_i-dependent weight factors:

$$[\nabla^2\Theta(\hat{\Omega})]_{lm} = \int \mathrm{d}\hat{\Omega}\, Y^*_{lm}(\hat{\Omega})[\nabla^2\Theta(\hat{\Omega})] = -l(l+1)\Theta_{lm}, \tag{34}$$

$$[\Theta^2(\hat{\Omega})]_{lm} = \int \mathrm{d}\hat{\Omega}\, Y^*_{lm}(\hat{\Omega})[\Theta^2(\hat{\Omega})] = \sum_{l_i m_i} (-1)^m \Theta_{l_1 m_1}\Theta_{l_2 m_2} I_{l_1 l_2 l} \begin{pmatrix} l_1 & l_2 & l \\ m_1 & m_2 & -m \end{pmatrix}, \tag{35}$$

$$\begin{aligned} [\nabla\Theta(\hat{\Omega})\cdot\nabla\Theta(\hat{\Omega})]_{lm} &= \int \mathrm{d}\hat{\Omega}\, Y^*_{lm}(\hat{\Omega})[\nabla\Theta(\hat{\Omega})\cdot\nabla\Theta(\hat{\Omega})] = \sum_{l_i m_i} \Theta_{l_1 m_1}\Theta_{l_2 m_2} \int \mathrm{d}\hat{\Omega}\, Y^*_{lm}(\hat{\Omega})[\nabla Y_{l_1 m_2}(\hat{\Omega})\cdot\nabla Y_{l_2 m_2}(\hat{\Omega})] \\ &= \frac{1}{3}\sum_{l_i m_i}[l_1(l_1+1)+l_2(l_2+1)-l(l+1)] \int \mathrm{d}\hat{\Omega}\, Y^*_{lm}(\hat{\Omega}) Y_{l_1 m_1}(\hat{\Omega}) Y_{l_2 m_2}(\hat{\Omega}) \\ &= = \frac{1}{3}\sum_{l_i m_i}(-1)^m [l_1(l_1+1)+l_2(l_2+1)-l(l+1)]\Theta_{l_1 m_1}\Theta_{l_2 m_2} I_{l_1 l_2 l} \begin{pmatrix} l_1 & l_2 & l \\ m_1 & m_2 & -m \end{pmatrix}. \end{aligned} \tag{36}$$

We can define the power spectrum associated with the MFs through the following third order expression:

$$V_k^{(3)} = \sum_l [V_k]_l (2l+1) = \frac{1}{6}\sum_l (2l+1)\left\{ S_l^{(0)} H(\nu) + \frac{k}{3} S_l^{(1)} H(\nu) + \frac{k(k-1)}{6} S_l^{(2)} H_{k-2}(\nu) + \cdots \right\}. \tag{37}$$

The 'three-skewness' defines the triplets of MFs. At the level of two-point statistics, in the harmonic domain we have three power spectra associated with MF $V_k^{(3)}$ that depend on the three skew-spectra we have defined. We will show later in this paper that the fourth-order correction terms also have a similar form, but with an additional monopole contribution that can be computed from the lower order one-point terms such as the three skewness defined here. The result presented here is important and implies that we can study the contributions to each of the MFs $v_k(\nu)$ as a function of harmonic mode l. This is an especially significant result as various forms of non-Gaussianity will have different l dependence and hence they can potentially be distinguished. The ordinary MFs add contributions from all individual l modes and hence have less power in differentiating various contributing sources of non-Gaussianity. This is one of main motivations for extending the concept of MFs (single numbers) to one-dimensional objects similar to the power spectrum. It is worth pointing out that the skewness, along with the generalized skewness parameters, is typically less sensitive to the background cosmology. They are more sensitive to the underlying model of non-Gaussianity. The main dependence on cosmology typically results from normalization coefficients, such as σ_0 and σ_1, which are determined using the power spectrum of tSZ.

In Fig. 3, we plot the three skew-spectra for a range of Gaussian beams with FWHM = 0–25 arcmin. We consider an ideal all-sky experimental set-up without any instrumental noise. The analytical results are computed using a halo model prediction for the bispectrum. The corresponding skew-spectra that include *Planck*-type noise are displayed in Fig. 4. As expected, the effect of noise is more pronounced at smaller angular scales. In Fig. 5, ideal noise-free all-sky results are plotted for the diffuse component. The bispectrum in this case is constructed using the perturbative approach. Fig. 6 shows the corresponding results for a *Planck*-type all-sky experiment. Notice that for near all-sky experiments the S/N degrades as $f_{\rm sky}$. All results shown are for $f_{\rm sky} = 1$.

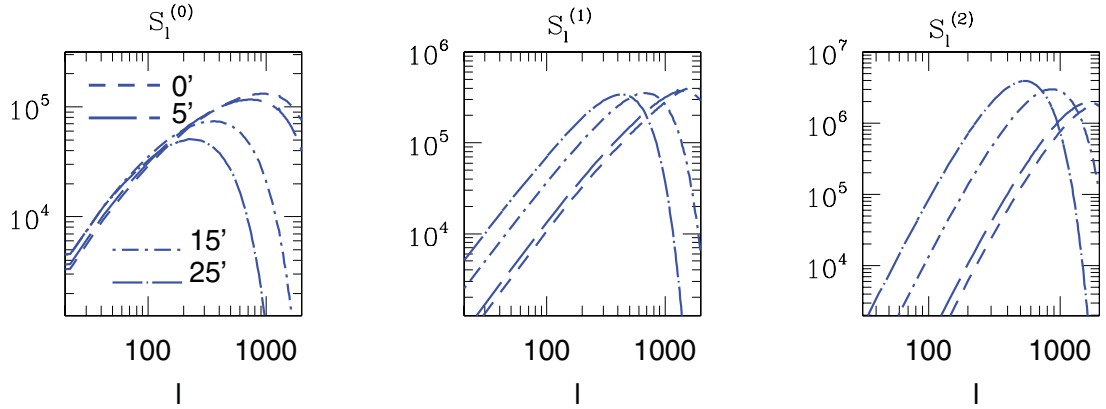

Figure 3. The absolute values of skew-spectra are plotted as a function of the harmonic l. From left to right the plots correspond to $S_l^{(0)}$, $S_l^{(0)}$ and $S_l^{(0)}$, respectively. We consider four different beams with FWHM = 0, 5, 15 and 25 arcmin, respectively, as indicated. These results correspond to *ideal noise-free* experiments, and the resolution is taken to be $l_{\rm max} = 2000$. The results are obtained using halo model prescription.

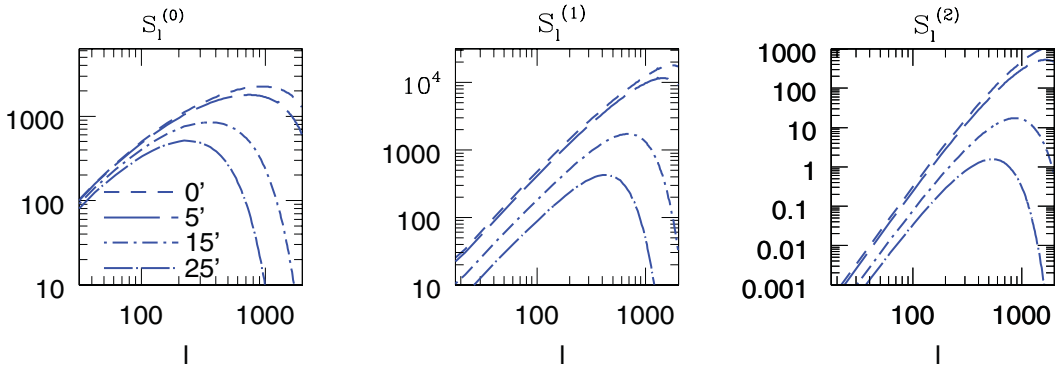

Figure 4. The absolute values of skew-spectra are plotted as a function of the harmonic l. From left to right the plots correspond to $S^{(0)}$, $S^{(1)}$ and $S^{(2)}$, respectively. We consider four different beams with FWHM = 0, 5, 15 and 25 arcmin, respectively, as indicated. These results include *Planck*-type noise and correspond to an all-sky survey.

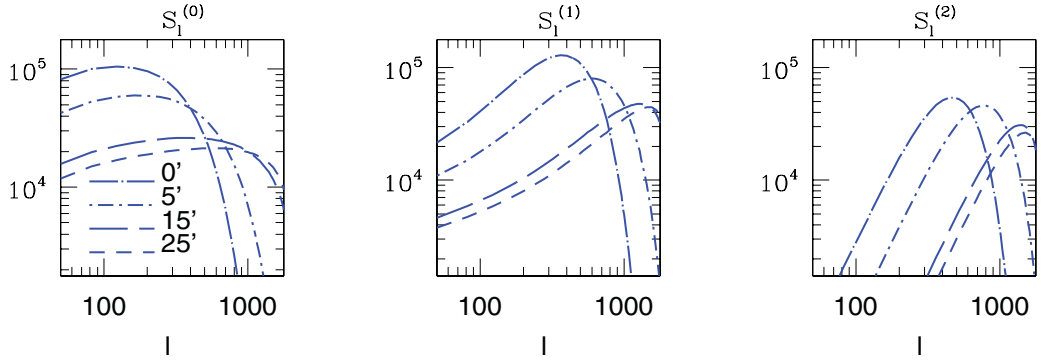

Figure 5. The skew-spectra are plotted as a function of the harmonic l. From left to right the plots correspond to $S_l^{(0)}$, $S_l^{(1)}$ and $S_l^{(2)}$, respectively. We consider four different beams with FWHM = 0, 5, 15 and 25 arcmin, respectively, as indicated. These results correspond to an ideal all-sky noise-free experiment. A perturbative calculation which assumes redshift-dependent linear biasing was used.

5 ESTIMATORS AND THEIR SCATTER

As we have noted before, the estimators for the skew-spectra can be most easily computed by cross-correlating maps in the harmonic domain. These maps are constructed in real space by applying various derivative operators. In the presence of masking, the recovered skew-spectra depend on the mask. The presence of a mask typically introduces mode–mode coupling. The approach we adopt here to reconstruct the unbiased power spectra in the presence of mask exploits the so-called pseudo-$\mathcal{C}_l$ (Hivon et al. 2002), which involves expressing the observed power spectra $\mathcal{C}_l$ in the presence of a mask as a linear combination of unbiased all-sky power spectra.

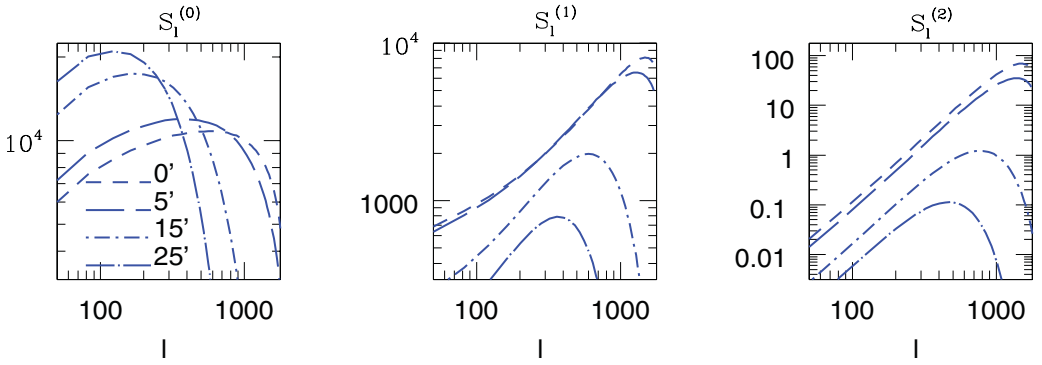

Figure 6. The skew-spectra are plotted as a function of the harmonic l. From left to right the plots correspond to $S^{(0)}$, $S^{(1)}$ and $S^{(2)}$, respectively. We consider four different beams with FWHM = 0, 5, 15 and 25 arcmin, respectively, as indicated. These results include *Planck*-type noise.

The three different generalized skew-spectra that we have introduced here can be thought as cross-spectra of relevant fields. We denote these generic fields by A and B and will denote the generic skew-spectra as $S_l^{A,B}$. The skew-spectra recovered in the presence of mask are represented as $\tilde{S}_l^{A,B}$, and the unbiased estimator is denoted by $\hat{S}_l^{A,B}$. The skew-spectra recovered in the presence of mask $\tilde{S}_l^{A,B}$ will be biased. However, to construct an unbiased estimator $\hat{S}_l^{A,B}$ for the skew-spectra, the following procedure is sufficient. The derivation follows the same arguments as detailed in Munshi et al. (2011a) and will not be reproduced here:

$$\tilde{S}_l^{A,B} = \frac{1}{2l+1}\sum_m \tilde{A}_{lm}\tilde{B}^*_{lm}, \quad \tilde{S}_l^{A,B} = \sum_{l'} M_{ll'} S_l^{A,B}, \quad M_{ll'} = \frac{1}{2l+1}\sum_{l'l''} I^2_{ll'l''}|w_{l''}|^2, \quad \{A,B\} \in \{\Theta, \Theta^2, (\nabla\Theta\cdot\nabla\Theta), \nabla^2\Theta\}. \tag{38}$$

In this notation we can write the skewness parameters defined previously as

$$S^{(0)} \equiv \mathrm{X}_{(0)} S_l^{(\Theta^2,\Theta)}, \quad S^{(1)} \equiv \mathrm{X}_{(1)} S_l^{(\Theta^2,\nabla^2\Theta)}, \quad S^{(2)} \equiv \mathrm{X}_{(2)} S_l^{(\nabla\Theta\cdot\nabla\Theta,\nabla^2\Theta)}, \qquad \{\mathrm{X}_{(0)}, \mathrm{X}_{(1)}, \mathrm{X}_{(2)}\} \equiv \left\{\frac{1}{12\pi\sigma_0^4}, \frac{1}{16\pi\sigma_0^2\sigma_1^2}, \frac{1}{8\pi\sigma_1^4}\right\}. \tag{39}$$

The mode–mode coupling matrix M is constructed from the power spectra of the mask $w_{l''}$ and used for estimation of unbiased skew-spectra $\hat{S}_{l''}^{A,B}$. Typically the mask consists of bright stars and saturated spikes where no lensing measurements can be performed. The results that we present here are generic. The estimator thus constructed is an unbiased estimator. The computation of covariance of the scatter in the estimates can be computed using analytical methods, thereby avoiding the need for expensive Monte Carlo simulations. The scatter or covariance of the unbiased estimates $\langle \delta\hat{S}_l^{A,B}\delta\hat{S}_{l'}^{A,B}\rangle$ is related to that of the direct estimates $\langle \delta\tilde{S}_l^{A,B}\delta\tilde{S}_{l'}^{A,B}\rangle$ from the masked sky by a similarity transformation. The transformation is given by the same mode coupling matrix M:

$$\hat{S}_l^{A,B} = \sum_{l'}[M^{-1}]_{ll'}\tilde{S}_{l'}^{A,B}, \quad \left\langle \delta\hat{S}_l^{A,B}\delta\hat{S}_{l'}^{A,B}\right\rangle = \sum_{LL'} M^{-1}_{lL}\left\langle \delta\tilde{S}_L^{A,B}\delta\tilde{S}_{L'}^{A,B}\right\rangle M^{-1}_{L'l'}, \quad \left\langle \hat{S}_l^{A,B}\right\rangle = S_l^{A,B}, \quad \{A,B\} \in \{\Theta, \Theta^2, (\nabla\Theta\cdot\nabla\Theta), \nabla^2\Theta\}. \tag{40}$$

The power spectra associated with the MFs are linear combinations of the skew-spectra (see equation 26). In our approach the power spectra associated with the MFs are secondary and can be constructed using the skew-spectra that are estimated directly from the data.

The construction of an estimator is incomplete without an estimate of its variance. The variance or the scatter in certain situation is computed using Monte Carlo simulations which are computationally expensive. In our approach, it is possible to compute the covariance of our estimates of various S_ls, i.e. $\langle \delta S_l \delta S_{l'}\rangle$ under the same simplifying assumptions that higher order correlation functions can be approximated as Gaussian. This allows us to express the error covariance in terms of the relevant power spectra. The generic expression can be written as

$$\left[\hat{V}_k^{(2)}\right]_l = \sum_{l'}[M^{-1}]_{ll'}\left[\tilde{V}_k^{(2)}\right]_{l'}, \qquad \left\langle \delta\hat{V}_k^{(2)}\delta\hat{V}_{k'}^{(2)}\right\rangle = \sum_{LL'} M^{-1}_{lL}\left\langle \delta[\tilde{V}_k^{(2)}]_l\delta[\tilde{V}_{k'}^{(2)}]_{l'}\right\rangle M^{-1}_{L'l'}. \tag{41}$$

We would like to point out here that, in case of limited sky coverage, it may not be possible to estimate the skew-spectra mode-by-mode as the mode coupling matrix may become singular and a broad binning of the spectra may be required:

$$\left\langle \left[\delta S_l^{X,Y}\right]\delta S_{l'}^{X,Y}]\right\rangle = f_{\rm sky}^{-1}\frac{1}{2l+1}\left[\mathcal{C}_l^{X,X}\mathcal{C}_{l'}^{Y,Y} + \left[S_l^{X,Y}\right]^2\right]\delta_{ll'}, \qquad \{X,Y\} \in \{\Theta, \Theta^2, \nabla\Theta(\hat{\Omega})\cdot\nabla\Theta(\hat{\Omega}), \nabla^2\Theta(\hat{\Omega})\}. \tag{42}$$

Here the fraction of sky covered by the survey is denoted by $f_{\rm sky}$. The expressions for the skew-spectra are quoted in $S_l^{(\Theta 2,\Theta)}$, $S_l^{(\kappa 2,\nabla 2\kappa)}$ and $S_l^{(\nabla\Theta\cdot\nabla\Theta,\nabla 2\Theta)}$ are given in equation (33). The expressions for covariance also depend on a set of power spectra, i.e. $S_l^{(\Theta 2,\Theta 2)}$, $S_l^{(\nabla 2\Theta,\nabla 2\Theta)}$, $S_l^{(\nabla\Theta\cdot\nabla\Theta,\nabla 2\Theta)}$ and $S_l^{\Theta,\Theta}$. These are given by the following expression:

$$\mathcal{C}_l^{\nabla\cdot\nabla,\nabla\cdot\nabla} = \sum_{l_1 l_2}\mathcal{C}^{\rm t}_{l_1}\mathcal{C}^{\rm t}_{l_2}[l_1(l_1+1)+l_2(l_2+1)-l(l+1)]^2 I^2_{ll_1l_2}, \quad \mathcal{C}_l^{[\Theta^2,\Theta^2]} = \sum_{l_1 l_2}\mathcal{C}^{\rm t}_{l_1}\mathcal{C}^{\rm t}_{l_2} I^2_{ll_1l_2}, \quad \mathcal{C}_l^{[\nabla^2\Theta,\nabla^2\Theta]} = l^2(l+1)^2\mathcal{C}^{\rm t}_l. \tag{43}$$

Here $\mathcal{C}^{\rm t}_l$ includes signal and noise power spectra $\mathcal{C}^{\rm t}_l = \mathcal{C}^S_l b_l^2 + \mathcal{C}^{\rm N}_l$. The experimental beam is denoted by b_l. Using these equations it is possible to compute the scatter in various skew-spectra. The scatter depends on the skew-spectra and various cross-spectra of combinations of product fields constructed from the original tSZ maps:

$$\left\langle \delta S_l^{[\Theta^2,\Theta]}\delta S_l^{[\Theta^2,\Theta]}\right\rangle = f_{\rm sky}^{-1}\frac{1}{2l+1}\left[\mathcal{C}_l^{[\Theta^2,\Theta^2]}\mathcal{C}_l^{[\Theta,\Theta]} + \left[S_l^{[\Theta^2,\Theta]}\right]^2\right], \tag{44}$$

$$\left\langle \delta S_l^{[\Theta^2,\nabla^2\Theta]} \delta S_l^{[\Theta^2,\nabla^2\Theta]} \right\rangle = f_{\rm sky}^{-1} \frac{1}{2l+1} \left[\mathcal{C}_l^{[\Theta^2,\Theta^2]} \mathcal{C}_l^{[\nabla\cdot\nabla,\nabla\cdot\nabla]} + \left[S_l^{[\Theta^2,\nabla^2\Theta]} \right]^2 \right], \tag{45}$$

$$\left\langle \delta S_l^{[\nabla\Theta\cdot\nabla\Theta,\nabla^2\Theta]} \delta S_l^{[\nabla\Theta\cdot\nabla\Theta,\nabla^2\Theta]} \right\rangle = f_{\rm sky}^{-1} \frac{1}{2l+1} \left[\mathcal{C}_l^{[\nabla^2\Theta,\nabla^2\Theta]} \mathcal{C}_l^{[\nabla\cdot\nabla,\nabla\cdot\nabla]} + \left[S_l^{[\nabla\Theta\cdot\nabla\Theta,\nabla^2\Theta]} \right]^2 \right]. \tag{46}$$

All relevant expressions for quantities used above are given in equation (43). The cumulative S/N up to a given $l_{\rm max}$ using these expression for estimators $S^{(0)}$ can now be expressed as

$$\left[({\rm S/N})^{(0)}_{l_{\rm max}} \right]^2 = f_{\rm sky} \sum_{l=2}^{l_{\rm max}} (2l+1) \left(S_l^{[\Theta^2,\Theta]} \right)^2 \Big/ \left[{\rm X}^2_{(0)} \mathcal{C}_l^{[\Theta^2,\Theta^2]} \mathcal{C}_l^{[\Theta,\Theta]} + \left[S_l^{[\Theta^2,\Theta]} \right]^2 \right], \tag{47}$$

$$\left[({\rm S/N})^{(1)}_{l_{\rm max}} \right]^2 = f_{\rm sky} \sum_{l=2}^{l_{\rm max}} (2l+1) \left(S_l^{[\Theta^2,\nabla^2\Theta]} \right)^2 \Big/ \left[{\rm X}^2_{(1)} \mathcal{C}_l^{[\Theta^2,\Theta^2]} \mathcal{C}_l^{[\nabla^2,\nabla^2]} + \left[S_l^{[\Theta^2,\nabla^2\Theta]} \right]^2 \right], \tag{48}$$

$$\left[({\rm S/N})^{(2)}_{l_{\rm max}} \right]^2 = f_{\rm sky} \sum_{l=2}^{l_{\rm max}} (2l+1) \left(S_l^{[\nabla\Theta\cdot\nabla\Theta,\nabla^2\Theta]} \right)^2 \Big/ \left[{\rm X}^2_{(2)} \mathcal{C}_l^{[\nabla^2\Theta,\nabla^2\Theta]} \mathcal{C}_l^{[\nabla\cdot\nabla,\nabla\cdot\nabla]} + \left[S_l^{[\nabla\Theta\cdot\nabla\Theta,\nabla^2\Theta]} \right]^2 \right]. \tag{49}$$

For the study of the tSZ effect we find that a robust determination of the generalized skew-spectra is possible for individual modes for almost the entire range of l values we have probed. This is important in differentiating them from other sources of non-Gaussianity. The skew-spectra are integrated statistics, meaning that their value at a given l depends on the entire range of l values probed. These results can also be extended to take into account the cross-correlation among various skew-spectra extracted from the same data:

$$\left\langle \delta S_l^{[\Theta^2,\Theta]} \delta S_l^{[\Theta^2,\nabla^2\Theta]} \right\rangle = f_{\rm sky}^{-1} \frac{1}{2l+1} \left[\mathcal{C}_l^{[\Theta^2,\Theta^2]} \mathcal{C}_l^{[\Theta,\nabla^2\Theta]} + S_l^{[\Theta^2,\nabla^2\Theta]} S_l^{[\Theta,\Theta^2]} \right], \tag{50}$$

$$\left\langle \delta S_l^{[\Theta^2,\Theta]} \delta S_l^{[\nabla\Theta\cdot\nabla\Theta,\nabla^2\Theta]} \right\rangle = f_{\rm sky}^{-1} \frac{1}{2l+1} \left[S_l^{[\Theta^2,\nabla^2\Theta]} \mathcal{C}_l^{[\Theta,\nabla\Theta\cdot\nabla\Theta]} + \mathcal{C}_l^{[\Theta^2,\nabla\Theta\cdot\nabla\Theta]} \mathcal{C}_l^{[\Theta,\nabla^2\Theta]} \right], \tag{51}$$

$$\left\langle \delta S_l^{[\Theta^2,\nabla^2\Theta]} \delta S_l^{[\nabla\Theta\cdot\nabla\Theta,\nabla^2\Theta]} \right\rangle = f_{\rm sky}^{-1} \frac{1}{2l+1} \left[\mathcal{C}_l^{[\Theta^2,\nabla\Theta\cdot\nabla\Theta]} \mathcal{C}_l^{[\nabla^2\Theta,\nabla^2\Theta]} + S_l^{[\Theta^2,\nabla^2\Theta]} S_l^{[\nabla^2\Theta,\nabla\Theta\cdot\nabla\Theta]} \right]. \tag{52}$$

This discussion involves the lowest order departure from Gaussianity in MFs using a third-order statistic, namely the bispectrum. The next-to-leading descriptions are characterized by the trispectrum, which is a fourth-order statistics. It is possible to extend the definition of skew-spectra to the case of kurt-spectra or the power spectrum associated with trispectrum. The power spectra associated with the MFs can be defined completely up to fourth order using the skew- and kurt-spectra. However, the corrections to leading order statistics from kurt-spectra are subdominant, and leading order terms are enough to study the departure from Gaussianity. It is nevertheless straightforward to implement an estimator which incorporates the power spectrum associated with the MFs from noisy data by including both third-order and fourth-order statistics. The issue has been dealt with in detail in Munshi, Smidt & Cooray (2010) in the context of the CMB sky.

In addition to the three generalized skew-spectra that define the MFs at lowest order in non-Gaussianity, it is possible to construct additional skew-spectra that work with different set of weights. In principle an arbitrary number of such skew-spectra can be constructed. Although they will not have direct links to the morphological properties that we have focused on, in this paper they can still be used as a source of independent information on the bispectrum, and can be used in principle to separate sources of non-Gaussianity, whether they be primordial or induced by late-time gravitational effects. In Fig. 7, we have plotted the S/N for the three skew-spectra for different choices of FWHM as indicated for an ideal experiment. The analytical results for the underlying bispectrum are obtained using the halo model prescription. The left-, middle and right-hand panels correspond to $S_l^{(0)}$, $S_l^{(1)}$ and $S_l^{(2)}$, respectively. In Fig. 8, the S/N for an all-sky experiment

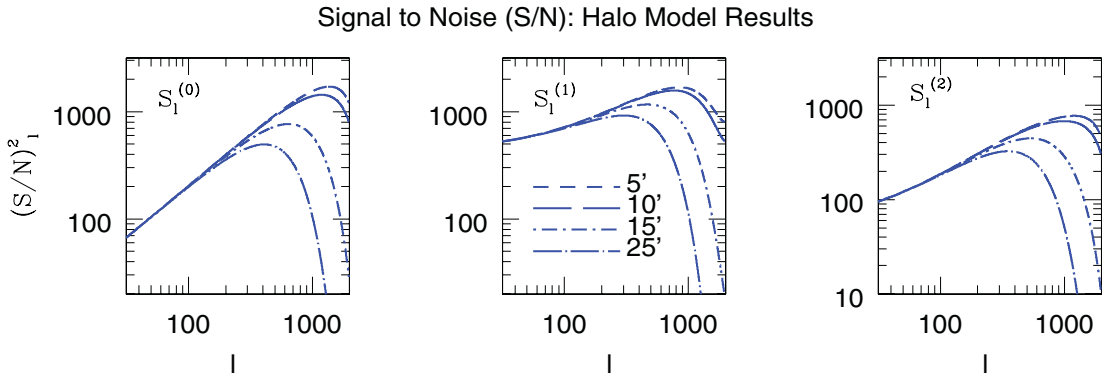

Figure 7. The S/N squared for various skew-spectra $S_l^{(0)}$ (left-hand panel), $S_l^{(1)}$ (middle panel) and $S_l^{(2)}$ (right-hand panel) are plotted as a function of angular harmonics l. We choose four different Gaussian beams with FWHM $\theta_{\rm s} = 0$, 5, 15, 25 arcmin. The higher resolution (smaller FWHM) reaches higher S/N. The plots correspond to an ideal experiment with all-sky coverage and no instrumental noise. The expressions used for computation of the S/N are given in equations (47)–(49). The results correspond to an ideal all-sky $f_{\rm sky} = 1$ *no-noise* set-up. For near all-sky experiments the S/N will scale directly with $f_{\rm sky}$.

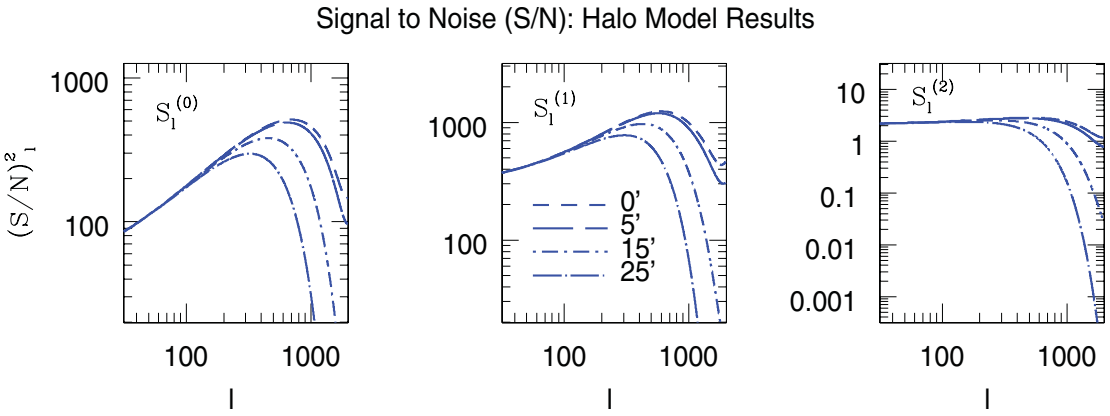

Figure 8. Same as Fig. 7 but with *Planck* noise added. Inclusion of noise degrades the S/N. The effect is most prominent for $S_l^{(2)}$ which is related to the fact that $S_l^{(2)}$ gives more weights to smaller scales than other estimates and hence more affected by the noise.

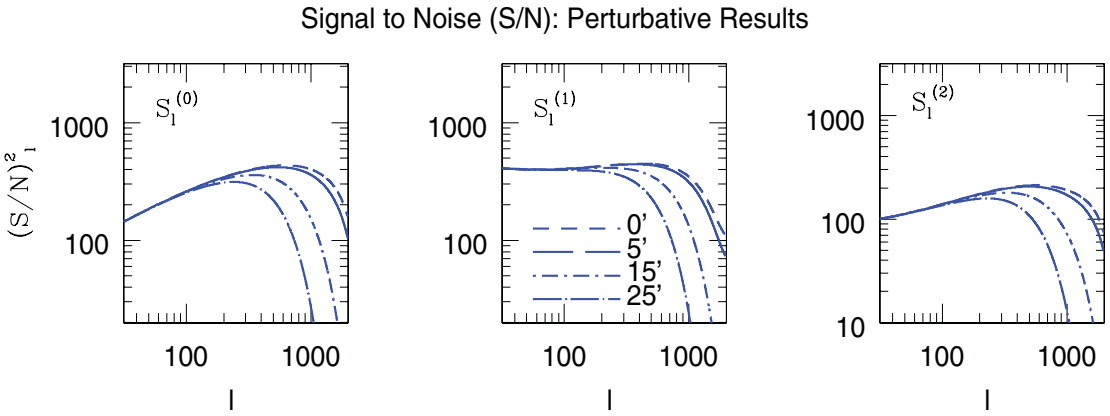

Figure 9. Same as Fig. 7 but for perturbative calculations. The perturbative bispectrum has less power at higher l compared to halo model calculations.

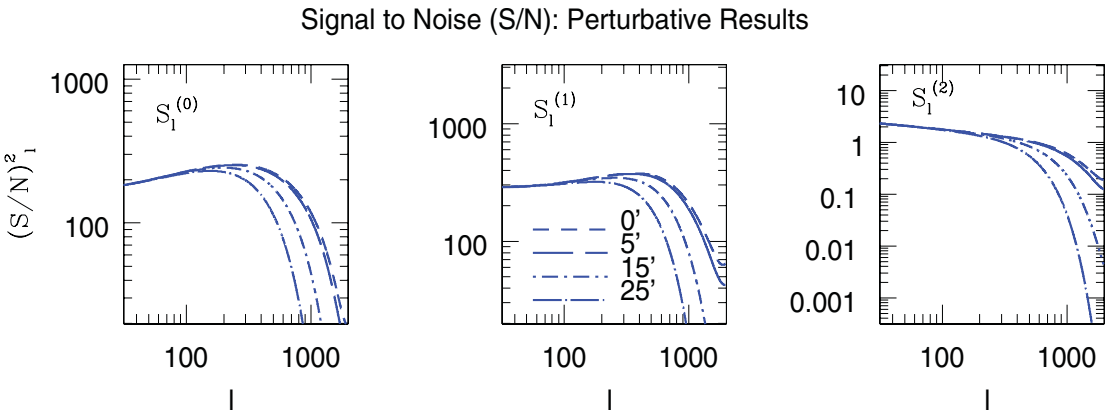

Figure 10. Results correspond to perturbative analysis but with instrumental noise for a *Planck*-type experiment included.

with *Planck*-type noise is shown. As expected the cases with smaller beam size have higher S/N. In Fig. 9, results for an ideal experiment are shown using perturbative calculations. We further show perturbative results that include *Planck*-type noise in Fig. 10. The skew-spectrum $S_l^{(2)}$ has the highest S/N among the three skew-spectra. The very high S/N will allow an accurate determination of all three spectra, in particular $S_l^{(0)}$ and $S_l^{(1)}$, for the entire range of l values probed.

6 CONCLUSION

In this study we have examined the prospects for extracting non-Gaussianity statistics originating from the tSZ effect via CMB surveys using MFs. The tSZ effect is associated with the hot gas in large-scale structure and is detectable by multifrequency experiments, in particular *Planck*. When compared with the CMB temperature anisotropies the tSZ effect has a distinct spectral signature which means it can be effectively

separated from the primary CMB contributions. This provides a unique opportunity to probe the tSZ effect using frequency-cleaned data in the near future. In the past, the statistical analysis of the frequency-cleaned tSZ maps has mainly been focused on lower order statistics. Morphological studies involving the MFs are complementary to the lower order statistics and carry independent information. In this paper we have generalized the study of MFs, typically used in cosmological contexts, in the case of tSZ maps.

As mentioned, the tSZ effect traces the fluctuations associated with the large-scale distribution of the baryonic gas. The generation of pressure fluctuations in virialized dark matter haloes can be modelled by assuming them to be in hydrostatic equilibrium with the dark matter distribution within the halo. The shock-heated gas typically corresponds to overdensities in excess of $\delta \geq 200$. The unshocked photoionized baryonic gas typically traces the large-scale distribution of the dark matter distribution. The usual overdensity in unshocked photoionized baryons is $\delta \leq 10$.

We have modelled the tSZ effect using two independent techniques. For smaller overdensities we employ a simplistic biasing model that relies on a perturbative description of dark matter clustering. The statistics of the hot gas is then linked to that of the dark matter using a linear (redshift dependent) biasing scheme. While this type of modelling is adequate for small overdensities, a more elaborate analytical scheme is required for a detailed description of baryonic clustering at smaller scales. We consider a halo-model-based approach for the gas in collapsed virialized haloes. The specific number density and radial profile of these haloes are modelled using Press–Schechter formalism or its variants. These two pictures of baryonic clustering are complementary to each other. The tSZ angular power spectrum corresponds to the projected power spectrum of the baryonic pressure fluctuations, and the tSZ angular bispectrum corresponds to the bispectrum of pressure fluctuations projected on to the surface of the sky.

Few comments on the validity of the perturbative results are in order. The tSZ power spectrum by and large depends on the one halo term in the halo modelling. However, in the perturbative regime we are mostly probing the Jeans-scale smoothed gas that is not in collapsed objects and which traces the smoothed large-scale dark matter distribution. To probe the large-scale SZ effect removing X-ray bright clusters can reduce contributions from collapsed haloes. Thus, the effect captured by the linear biasing scheme should be understood as a signal in blank fields where such clusters are absent. It provides the lower limit of SZ effect from the large-scale structure distribution. Though the diffuse component of the tSZ effect is beyond *WMAP* detection threshold the situation may improve with future data sets such as *Planck* (Hansen et al. 2005; also see Joudaki et al. 2010).

The tSZ effect is intrinsically non-Gaussian. While the tSZ power spectrum is sensitive to the amplitude of the density fluctuations, higher order statistics such as skewness of the tSZ effect can be used to separate the pressure bias from the amplitude of the density fluctuations because the skewness is related to the bispectrum of the tSZ effect. The individual modes of a specific bispectrum, defined by triplets of the harmonic numbers (l_1, l_2, l_3), have low S/N and may not be easy to estimate from noisy data. In a recent study, Munshi & Heavens (2010) advocated using spectra related to the higher order polyspectra particularly the bispectrum; the skew-spectrum is the lowest such spectrum that is constructed from the bispectrum. The skew-spectra retain some of the shape dependence of the bispectrum without compressing it to a single number. The three different skew-spectra we used in this paper are generalizations of the ordinary skew-spectrum that was first introduced in Munshi & Heavens (2010), and later used in the context of weak lensing and CMB for morphological analysis. These three different skew-spectra can also be used to study the morphology of the tSZ maps as described by the MFs. They associate varying weights to individual bispectrum modes when constructing the skew-spectra and carry independent information.

Using a nearly full sky framework and noise that reflects ongoing CMB observations such as *Planck* we have studied how well the three different skew-spectra can be estimated from data. We find that the data will allow a *robust* determination of two of the three skew-spectra that we have considered with very high level of S/N. This is true for both perturbative results and the results that are based on the halo model for the entire range of angular smoothing scales that we have studied. We also find the estimation of $S^{(2)}$ will be dominated by noise. The high S/N for the other two power spectra will allow mode-by-mode estimation of each skew-spectrum. This can help to distinguish them from other sources of non-Gaussianity.

The method that we pursue here depends on having access to frequency-cleaned tSZ maps. The tSZ effect can also be studied using cross-correlation techniques that involve external tracers. Such methods typically employ mixed bispectra. However, the results lack frequency information and are typically confusion-noise dominated. The study of tSZ using the bispectrum from frequency-cleaned maps typically provides additional S/N due to the frequency information. In the absence of frequency information the background CMB plays the role of intrinsic noise that degrades the S/N. It is also interesting to note that removal of tSZ from CMB maps may actually help in the detection of other subdominant effects that we have not studied here, such as the kinetic SZ effect.

Some of the techniques described here will have wider applicability. The idea of generalized skew-spectra was shown to be useful in the context of weak lensing surveys (Munshi et al. 2011b) and primordial non-Gaussianity from CMB maps (Munshi et al. 2010). In this study, we have concentrated on the leading order terms in the construction of the power spectra associated with the MFs. However, the next-to-leading order terms can also be taken into account with the same formalism. The next-to-leading order terms will involve kurt-spectra that generalize the concept of skew-spectra at fourth order. The four quadruplets of generalized kurt-spectra are related to the trispectrum in a way that is similar to the relationship of skew-spectra and the bispectrum we have considered in this paper. The generalized kurt-spectra and the related generalized kurtosis can be extracted from the data using the same PCL approach we have discussed here. However, the correction to generalized skew-spectra associated with MFs resulting from the trispectrum is expected to be negligible compared to the leading contribution from the generalized skew-spectra.

ACKNOWLEDGMENTS

DM acknowledges support from STFC standard grant ST/G002231/1 at School of Physics and Astronomy at Cardiff University where this work was completed. SJ and JS acknowledge support from the US Department of Education through GAANN fellowships at UCI. It is a pleasure for DM to thank Alan Heavens, Patrick Valageas and Ludo van Waerbeke for many useful discussions.

REFERENCES

Aghanim N., Majumdar S., Silk J., 2008, Rep. Progress Phys., 71, 066902
Bernardeau F., Colombi S., Gaztanaga E., Scoccimarro R., 2002, Phys. Rep., 367, 1
Birkinshaw M., 1999, Phys. Rep., 310, 98
Bouchet F. R., Gispert R., 1999, New Astron., 4, 443
Bouchet F. R., Juszkiewicz R., Colombi S., Pellat R., 1992, ApJ, 394, L5
Cao L., Liu J., Fang L.-Z., 2007, ApJ, 661, 641
Cen R., Ostriker J. P., 1999, ApJ, 514, 1
Cooray A., 2000, Phys. Rev. D, 62, 103506
Cooray A., 2001a, Phys. Rev. D, 64, 043516
Cooray A., 2001b, Phys. Rev. D, 64, 063514
Cooray A., Seth R., 2002, Phys. Rep., 372, 1
Cooray A., Hu W., Tegmark M., 2000, ApJ, 540, 1
Cooray A., Baumann D., Sigurdson K., 2005, in Melchiorri F., Rephaeli Y., eds, Proceedings of the International School of Physics 'Enrico Fermi', Background Microwave Radiation and Intracluster Cosmology. IOS Press, Bologna, p. 309
da Silva A. C., Barbosa D., Liddle A. R., Thomas P. A., 2000, MNRAS, 317, 37
Delabrouille J., Cardoso J., Patanchon G., 2003, MNRAS, 330, 807
Edmonds A. R., 1968, Angular Momentum in Quantum Mechanics, 2nd edn. Princeton Univ. Press, Princeton, NJ
Fry J. N., 1984, ApJ, 279, 499
Goldberg D. M., Spergel D. N., 1999a, Phys. Rev. D, 59, 103001
Goldberg D. M., Spergel D. N., 1999b, Phys. Rev. D, 59, 103002
Hadwiger H., 1959, Math. Z., 71, 124
Hallman E. J., O'Shea B. W., Burns J. O., Norman M. L., Harkness R., Wagner R., 2007, ApJ, 671, 27
Hallman E. J., O'Shea B. W., Smith B. D., Burns J. O., Norman M. L., 2009, ApJ, 698, 1759
Hansen F., Branchini E., Mazzotta P., Cabella P., Dolag K., 2005, MNRAS, 361, 753
Hikage C. et al., 2002, PASJ, 54, 707
Hikage C., Taruya A., Suto Y., 2003a, PASJ, 55, 335
Hikage C. et al., 2003b, PASJ, 55, 911
Hikage C., Komatsu E., Matsubara T., 2006, ApJ, 653, 11
Hikage C., Coles P., Grossi M., Moscardini L., Dolag K., Branchini L., Matarrese S., 2008, MNRAS, 385, 1513
Hivon E., Górski K. M., Netterfield C. B., Crill B. P., Prunet S., Hansen F., 2002, ApJ, 567, 2
Hui L., 1999, ApJ, 519, L9
Joudaki S., Smidt J., Amblard A., Cooray A., 2010, J. Cosmol. Astropart. Phys., 1008, 027
Komatsu E., Seljak U., 2002, MNRAS, 336, 1256
Leach S. M. et al., 2008, A&A, 491, 597
Limber D. N., 1954, ApJ, 119, 665
Lin K.-Y., Woo T.-P., Tseng Y.-H., Lin L., Chiueh T., 2004, ApJ, 608, L1
LoVerde M., Afshordi N., 2008, Phys. Rev. D, 78, 123506
Mo H. J., White S. D. M., 1996, MNRAS, 282, 347
Mo H. J., Jing Y. P., White S. D. M., 1997, MNRAS, 284, 189
Munshi D., Heavens A., 2010, MNRAS, 401, 2406
Munshi D., Smidt J., Cooray A., 2010, preprint (arXiv:1011.5224)
Munshi D., Heavens A., Cooray A., Valageas P., 2011a, MNRAS, 414, 3173
Munshi D., van Waerbeke L., Smidt J., Coles P., 2011b, preprint (arXiv:1103.1876)
Navarro J., Frenk C., White S. D. M., 1996, ApJ, 462, 563
Peebles P. J. E., 1971, Physical Cosmology. Princeton Univ. Press, Princeton, NJ
Persi F., Spergel D., Cen R., Ostriker J., 1995, ApJ, 442, 1
Press W., Sechter P., 1974, ApJ, 187, 425
Refregier A., Teyssier R., 2002, Phys. Rev. D, 66, 043002
Refregier A., Komatsu E., Spergel D. N., Pen U.-L., 2000, Phys. Rev. D, 61, 123001
Rephaeli Y., 1995, ARA&A, 33, 541
Roncarelli M., Moscardini L., Borgano S., Dolag K., 2007, MNRAS, 378, 1259
Runyan M. C. et al., 2003, ApJS, 149, 265
Scoccimarro R., Couchman H. M. P., 2001, MNRAS, 325, 1312
Scoccimarro R., Frieman J. A., 1999, ApJ, 520, 35
Seljak U., 2000, MNRAS, 318, 203
Seljak U., Burwell J., Pen U.-L., 2001, Phys. Rev. D, 64, 063001
Smidt J., Joudaki S., Serra P., Amblard A., Cooray A., 2010, Phys. Rev. D, 81, 123528
Springel V., White M., Hernquist L., 2001, ApJ, 549, 681
Sunyaev R. A., Zel'dovich Ya B., 1972, Comments Astrophys. Space Phys., 4, 173

Sunyaev R. A., Zel'dovich Ya B., 1980, ARA&A, 18, 537
The Planck Collaboration, 2006, preprint (astro-ph/0604069)
Veneziani M. et al., 2009, ApJ, 702, L61
White M., Hernquist V., Springel V., 2002, ApJ, 579, 16
Zhang P., Pen U.-L., 2001, ApJ, 549, 18
Zhang P., Seth R. K., 2007, ApJ, 579, 16
Zhang P., Pen U.-L., Trac H., 2004, MNRAS, 355, 451

This paper has been typeset from a TEX/LATEX file prepared by the author.